ISSN 1063-7761, Journal of Experimental and Theoretical Physics, 2018, Vol. 126, No. 5, pp. 683–698. © Pleiades Publishing, Inc., 2018.
Original Russian Text © E.I. Shneyder, I.A. Makarov, M.V. Zotova, S.G. Ovchinnikov, 2018, published in Zhurnal Eksperimental'noi i Teoreticheskoi Fiziki, 2018, Vol. 153, No. 5, pp. 820–837.

ELECTRONIC PROPERTIES OF SOLID

Influence of the Diagonal and Off-Diagonal Electron–Phonon Interactions on the Formation of Local Polarons and Their Band Structure in Materials with Strong Electron Correlations

E. I. Shneyder[a,b,*], I. A. Makarov[a], M. V. Zotova[a,b], and S. G. Ovchinnikov[a,b]

[a] *Kirensky Institute of Physics, Federal Research Center "Krasnoyarsk Scientific Center," Siberian Branch, Russian Academy of Sciences, Akademgorodok 50, Krasnoyarsk, 660036 Russia*

[b] *Federal State Autonomous Higher-Education Enterprise Siberian Federal University, pr. Svobodnyi 79, Krasnoyarsk, 660041 Russia*

**e-mail: shneyder@iph.krasn.ru*

Received October 20, 2017

Abstract—For systems with strong electron correlations and strong electron–phonon interaction, we analyze the electron–phonon interaction in local variables. The effects of the mutual influence of electron–electron and electron–phonon interactions that determine the structure of local Hubbard polarons are described. Using a system containing copper–oxygen layers as an example, we consider the competition between the diagonal and off-diagonal interactions of electrons with the breathing mode as the polaron band structure is formed within a corrected formulation of the polaron version of the generalized tight-binding method. The band structure of Hubbard polarons is shown to depend strongly on the temperature due to the excitation of Franck–Condon resonances. For an undoped La_2CuO_4 compound we have described the evolution of the band structure and the spectral function from the hole dispersion in an antiferromagnetic insulator at low temperatures with the valence band maximum at point $(\pi/2, \pi/2)$ to the spectrum with the maximum at point (π, π) typical for the paramagnetic phase. The polaron line width at the valence band top and its temperature dependence agree qualitatively with angle-resolved photoemission spectroscopy for undoped cuprates.

DOI: 10.1134/S1063776118050059

1. INTRODUCTION

Developing the ideas of such materials as high-temperature superconducting cuprates and many other transition metal oxides (manganites, cobaltites, etc.) combined under the term "systems with strong electron correlations" requires a proper allowance for not only the effects of local Coulomb electron–electron interaction but also strong electron–phonon interaction (EPI). As a rule, such systems are studied in the simplest case in the Hubbard model or the low-energy effective t–J model; more realistic approaches are based on the multiband p–d model or its reduction to a single-band Hamiltonian. In this case, the phonon subsystem and the electron–phonon interaction are described in terms of the Holstein Hamiltonian [1, 2] with a constant coupling constant $g(\mathbf{k}, \mathbf{q}) = g$ and dispersionless modes $\omega_{\mathbf{q}} = \omega$ or in terms of the Fröhlich Hamiltonian [3] with a coupling constant $g(\mathbf{k}, \mathbf{q}) \sim 1/q$ as well as in terms of modified Hamiltonians with coupling constants that take into account the peculiarities of the interaction [4–17]. (Here, $\mathbf{k}$ and $\mathbf{q}$ are the initial electron momentum and the transferred phonon momentum, respectively.)

The interaction of electronic excitations with lattice ones is considered in various ways, depending on the EPI strength. If lattice vibrations change significantly the electron spectrum, then polarons are said to be formed and the bound state of electrons and phonons is investigated. Otherwise, the interaction of electrons with phonons is described in terms of the perturbation theory, i.e., by assuming that the already formed quasiparticles interact with the lattice. Allowance should be made for the fact that in strongly correlated systems the electronic quasiparticle excitations differ from the Fermi-liquid ones: in view of the strong local Coulomb interaction between electrons, the two-particle states turn out to be pushed out into the high-energy part of the spectrum. This leads to a redistribution of the spectral weight between single- and two-particle excitations and, as a consequence, to significant peculiarities of the electronic structure of the material. The corresponding quasiparticle excitations are called Hubbard fermions.

The interaction of formed Hubbard fermions with phonons was considered previously in [18], also in the scheme of the generalized tight-binding method [19, 20], where the transition to the corresponding low-

energy Hamiltonian was made [19]. In this paper we will discuss the formation and properties of quasiparticle excitations due to the simultaneous strong influence of electron–electron and electron–phonon interactions. Such a statement of the problem is relevant for undoped and weakly doped cuprates as well as for many other Mott–Hubbard 3*d*-oxides-insulators in the regime of strong coupling between the electron and phonon subsystems.

The inapplicability of the adiabatic approach and single-electron approximations suggests a search for new ways of description. The proposed method is based on the assumption that the renormalizations of electronic excitations by the Coulomb and electron–phonon interactions are attributable primarily to their local part. The procedure of the method is such that when the quasiparticle excitations are determined, the local and nonlocal effects of electron–electron and electron–phonon interactions are taken into account exactly and within the approximation chosen for the problem under consideration, respectively.

The subsequent plan of the paper is as follows. A consistent derivation of the EPI Hamiltonian for systems with strong electron correlations in local variables is considered in Section 2. The role of competition between the diagonal and off-diagonal EPI for the breathing mode during the formation of local CuO-cluster states is analyzed in Section 3. For the convenience of the readers, the ideology and the computational scheme of the polaron version of the generalized tight-binding method taking into account the temperature effects are briefly outlined in Section 4. The band structure and the spectral weight of Hubbard polarons at finite temperatures are presented in Section 5. A discussion of the results and our conclusions are contained in Section 6.

2. ANALYSIS OF THE ELECTRON–PHONON INTERACTION FOR STRONGLY CORRELATED SYSTEMS IN LOCAL VARIABLES

When choosing the initial Hamiltonian, we will take into account the fact that in systems with strong electron correlations (SECs) the quasiparticle excitations can possess the properties of a Hubbard fermion and a polaron simultaneously. In the polaron version of the generalized tight-binding method we call such quasiparticles Hubbard polarons. Their dispersion is determined by the hybridization of Hubbard fermion bands with local Franck–Condon resonances [21]. Despite the fact that the characteristic scales of the electronic structure in cuprates exceed appreciably the frequencies of vibrational modes strongly interacting with electrons, renormalizations of the electronic structure over the entire depth of not only the valence band but also the conduction band emerge at a sufficient EPI strength [21]. In other words, elementary quasiparticle excitations are formed outside the low-energy windows of effective single-band Hamiltonians. In this case, an adequate description and subsequent construction of the corresponding effective Hamiltonians must be based on the approaches that start from realistic models and take into account the electron–electron and electron–phonon interactions on an equal footing. One of such approaches was proposed previously in [22] and was developed in [21] within the generalized tight-binding (GTB) method. In this section we will refine the formulation of the polaron version of this method by performing a consistent analysis of the EPI for systems with SECs in local variables.

Since the choice of a Hamiltonian for the electron subsystem also depends on what vibrations will be taken into consideration, we will begin with a discussion of the modes that are the sources of the strongest EPI in cuprates. As is well known [23, 24], first, the high-energy modes changing the oxygen–copper hopping integrals and, thus, modulating a high Zhang–Rice singlet energy belong to them. These are the breathing and half-breathing vibrations of oxygen atoms in the CuO plane. Second, these are the buckling and tilting modes involving the in-phase or out-of-phase vibrations of planar oxygen atoms across the CuO plane along the *c* axis. Some of them are related to the instability of the system with respect to the structural phase transition. Finally, these include the modes characterized by the motions of an apical oxygen atom along the *c* axis (apical breathing). Their strong coupling with electrons [25] is attributable to weak screening of the electrostatic Coulomb interaction in this direction. All of the listed vibrations exhibit various anomalies of the phonon spectra pointing to their strong interaction with electrons in certain doping and temperature ranges [26–28].

For our model description of the EPI in the polaron version of the GTB method, we will take into account the optical, so-called planar, breathing mode. It is present in all parent compounds of high-T_c cuprates. Its dominant contribution to the total electron–phonon coupling constant has been repeatedly demonstrated in various approximations [6, 29, 30]. For example, when estimating the EPI effects in cuprates based on first-principles calculations and the Migdal approximation, Giustino et al. [31] showed that for an optimally doped compound the contribution of breathing planar modes to the real part of the electron self-energy due to the their interaction with phonons is dominant [31].

In contrast to the breathing mode, the contribution to the electron–phonon interaction from the buckling and tilting modes in the first order in displacements arises either from the distortion of CuO planes or in the presence of a finite electric field along the *c* axis due to, for example, the asymmetric environment of the CuO-plane atoms [5]. In addition, allowance for the buckling vibrations requires attention to the anhar-

monicity effects [32]. In contrast, the breathing vibrations of apical oxygen atoms are apparently of no crucial importance in describing the electronic structure and some properties of cuprates due to the orthogonality of the phonon wave vector and the electron momentum in the CuO plane [7, 33]. This conclusion is confirmed by the experiments on site-selective oxygen isotope substitution [34] pointing to a dominant contribution of the planar oxygen atoms in the isotope shift of the critical temperature T_c.

To describe the interaction of CuO-plane electrons with the longitudinal breathing mode, let us consider the following Hamiltonian:

$$H = H^{\mathrm{el}} + H^{\mathrm{ph}} + H^{\mathrm{epi}}, \tag{1}$$

where H^{el} is the Hamiltonian of the realistic three-band p–d model of cuprates including all relevant interactions in the CuO plane:

$$\begin{aligned} H^{\mathrm{el}} &= \sum_{\mathbf{g},\sigma}(\varepsilon_d - \mu)n^d_{\mathbf{g},\sigma} + \sum_{\mathbf{g}} U_d n^d_{\mathbf{g},\sigma} n^d_{\mathbf{g},-\sigma} \\ &+ \sum_{\mathbf{g},\delta,\sigma}(\varepsilon_p - \mu)n^p_{\mathbf{g}+\delta,\sigma} + \sum_{\mathbf{g},\delta} U_p n^p_{\mathbf{g}+\delta,\sigma} n^p_{\mathbf{g}+\delta,-\sigma} \\ &+ \sum_{\langle \mathbf{g},\mathbf{g}'\rangle,\delta,\sigma} P_{\delta\delta'} t_{pp}(p^\dagger_{\mathbf{g}+\delta,\sigma} p_{\mathbf{g}'+\delta',\sigma} + \mathrm{H.c.}) \\ &+ \sum_{\mathbf{g},\delta,\sigma} P_\delta t_{pd}(d^\dagger_{\mathbf{g},\sigma} p_{\mathbf{g}+\delta,\sigma} + \mathrm{H.c.}) \\ &+ \sum_{\mathbf{g},\delta,\sigma,\sigma'} V_{pd} n^p_{\mathbf{g}+\delta,\sigma} n^d_{\mathbf{g},\sigma'}. \end{aligned} \tag{2}$$

Here, the vectors $\mathbf{g}$ number the copper sites and the vectors $\mathbf{g} + \delta$ specify the positions of the surrounding oxygen atoms. The quantities ε_d and ε_p are the local energies of the copper and oxygen atomic orbitals, $n^d_{\mathbf{g},\sigma} = d^\dagger_{\mathbf{g},\sigma} d_{\mathbf{g},\sigma}$ and $n^p_{\mathbf{g}+\delta,\sigma} = p^\dagger_{\mathbf{g}+\delta,\sigma} p_{\mathbf{g}+\delta,\sigma}$ are the corresponding number operators for particles (holes) with spin σ, t_{pp} and t_{pd} are the overlap integrals of these orbitals, μ is the chemical potential, U_d and U_p are the intraatomic Coulomb matrix elements, and V_{pd} is the interatomic one. The phase factors $P_{\delta\delta'}$ and P_δ are equal to ± 1, depending on whether the orbitals (with real wave functions) have identical or opposite signs in the overlap region.

We will write the Hamiltonians of the phonon system and the electron–phonon interaction at this stage in the most general case by noting that for optical phonons the deformation potential is proportional simply to the displacements of atoms:

$$H^{\mathrm{ph}} = \sum_{\mathbf{q}s} \hbar\omega_{\mathbf{q}s}\left(f^\dagger_{\mathbf{q}s} f_{\mathbf{q}s} + \frac{1}{2}\right), \tag{3}$$

$$H^{\mathrm{epi}} = \sum_{\nu,\zeta,\zeta'} M(\nu,\zeta,\zeta')(f^\dagger_{-\nu} + f_\nu)c^\dagger_\zeta c_{\zeta'}, \tag{4}$$

where $\zeta = (\mathbf{k}, \gamma, \sigma)$, $\nu = (\mathbf{q}, s)$, and $-\nu = (-\mathbf{q}, s)$. The operators $f^\dagger_\nu(f_\nu)$ and $c^\dagger_\nu(c_{\zeta'})$ describe, respectively, the creation (annihilation) of an s-branch phonon with momentum $\mathbf{q}$ and frequency $\omega_{\mathbf{q}s}$ or an electron with band index γ, momentum $\mathbf{k}$, and spin σ. The wave vectors $\mathbf{k}$, $\mathbf{k}'$, and $\mathbf{q}$ are related by the energy conservation law. Finally, $M(\nu, \zeta, \zeta')$ is the EPI matrix element.

Out of all possible processes of energy exchange between the subsystems of electrons and phonons, we will take into account only the largest contributions for one breathing mode in Eq. (4). These are the terms related to the modulation of the hopping parameter t_{pd} and the local energy ε_d of electrons on copper atoms (the charge density displacement type of electron–phonon interaction). They are also called transitive (or off-diagonal) and local (or diagonal) EPI in the literature, respectively. Due to the obvious competition between these two contributions, it is important to consider their combined influence on the system's characteristics. For a separate molecule the latter contribution is responsible only for the vibration frequency renormalization as the electron occupation numbers change [35]. In contrast, in a lattice energy is exchanged between phonons and d electrons. The small overlap between the orbitals of neighboring copper ions allows us not to describe the corresponding hopping in the electron Hamiltonian, while the mass of the copper atoms, much larger than the mass of the oxygen atoms, allows the copper displacements to be neglected. At the same time, the change in the crystal field on copper may turn out to be significant for a strongly correlated system, because it leads to a change in the energy of quasiparticle excitations, which, as a result, determine the electronic structure and, hence, this contribution requires an analysis.

Suppose that the mode under consideration is dispersionless. In the site representation Eqs. (3) and (4) will then take a simple form:

$$H^{\mathrm{ph}} = \sum_g \hbar\omega\left(f^\dagger_g f_g + \frac{1}{2}\right), \tag{5}$$

$$\begin{aligned} H^{\mathrm{epi}} &= \sum_{\mathbf{g},\sigma} M_d(f^\dagger_{\mathbf{g}} + f_{\mathbf{g}})d^\dagger_{\mathbf{g}\sigma} d_{\mathbf{g}\sigma} \\ &+ \sum_{\mathbf{g},\delta,\sigma} M_{pd} P_\delta (f^\dagger_{\mathbf{g}} + f_{\mathbf{g}})(d^\dagger_{\mathbf{g}\sigma} p_{\mathbf{g}+\delta,\sigma} + \mathrm{H.c.}). \end{aligned} \tag{6}$$

To implement the procedure [36, 37] of the GTB method, the total Hamiltonian (1) should be divided into the intracluster and intercluster parts, solving the concomitant problem of orthogonalization of the molecular orbitals of the neighboring cells. This will allow us to find exact solutions for the CuO_4 cluster, to pass to the Hubbard operator representation on their basis, and then to take into account the intercluster interaction via the perturbation theory. It is important that the system's characteristics determined in this way will contain the effects of both strong local Cou-

lomb interaction and EPI already in the zeroth approximation of the perturbation theory.

The orthogonalization problem for the electron Hamiltonian was solved by Shastry [38] through the introduction of "canonical" fermions. A detailed description of this procedure for a multiband p–d model within the GTB method is presented in [36]. The authors of [22] suggested using a similar approach for the EPI Hamiltonian as well. While developing this idea, we will correct its formulation in accordance with the general approaches to the EPI in crystals [39].

Let us consider in detail the off-diagonal contribution H_{pd}^{epi} to the EPI in Eq. (6) and take into account the relation of the phonon field operators to the phonon displacement operator. For one dispersionless mode we have

$$\sqrt{\frac{\hbar}{2m\omega}}(f_{\mathbf{g}}^{\dagger} + f_{\mathbf{g}}) = Q_{\mathbf{g}},$$

where m is the mass of the oxygen atom. On the other hand, the normal coordinate $Q_{\mathbf{g}}$ of the planar breathing vibrations corresponds to the following superposition of the displacements of oxygen atoms:

$$Q_{\mathbf{g}} = \frac{1}{2}\sum_{\alpha}(U_{\mathbf{g}+\mathbf{a}_{\alpha}/2} - U_{\mathbf{g}-\mathbf{a}_{\alpha}/2}). \tag{7}$$

Here, $\alpha = x$, y and $\mathbf{a}_{\alpha}$ are the unit-cell vectors. The choice of the signs before the displacements corresponds to an EPI constant $M_{pd} > 0$ and shows that the overlapping integral t_{pd} decreases with increasing Cu–O bond length. Let us introduce auxiliary bosonic operators for each displacement,

$$U_{\mathbf{g}\pm\mathbf{a}_{\alpha}/2} = \sqrt{\frac{\hbar}{2m\omega}}(e_{\mathbf{g}\pm\mathbf{a}_{\alpha}/2}^{\dagger} + e_{\mathbf{g}\pm\mathbf{a}_{\alpha}/2}), \tag{8}$$

and simplify the notation by combining the operators in pairs in such a way that

$$e_{\alpha,\mathbf{g}}^{\dagger} = e_{\mathbf{g}+\mathbf{a}_{\alpha}/2}^{\dagger} - e_{\mathbf{g}-\mathbf{a}_{\alpha}/2}^{\dagger},$$

$$p_{\alpha,\mathbf{g}} = p_{\mathbf{g}-\mathbf{a}_{\alpha}/2} - p_{\mathbf{g}+\mathbf{a}_{\alpha}/2}.$$

The Hamiltonian of the off-diagonal electron–phonon interaction will then take the form

$$H_{pd}^{\text{epi}} = \frac{1}{2}\sum_{\mathbf{g},\alpha,\alpha',\sigma} M_{pd}(e_{\alpha,\mathbf{g}}^{\dagger} + e_{\alpha,\mathbf{g}})(d_{\mathbf{g}\sigma}^{\dagger}p_{\alpha',\mathbf{g},\sigma} + \text{H.c.}). \tag{9}$$

Here, we took into account the phase factors P_{δ} by reconciling their choice with [36]. Finally, let us perform the Fourier transform in the last expression by noting that for the operators that are not centered on copper sites they obey the following rule:

$$e_{\mathbf{g}\pm\mathbf{a}_{\alpha}/2} = \frac{1}{\sqrt{N}}\sum_{\mathbf{q}} e_{\alpha,\mathbf{q}} \exp\left[-i\mathbf{q}\left(\mathbf{g} \pm \frac{\mathbf{a}_{\alpha}}{2}\right)\right].$$

As a result, we will obtain

$$\begin{aligned} H_{pd}^{\text{epi}} &= 2\sum_{\mathbf{k},\mathbf{q},\sigma} M_{pd}(e_{x,\mathbf{q}}^{\dagger}s_{x,\mathbf{q}} + e_{y,\mathbf{q}}^{\dagger}s_{y,\mathbf{q}} + \text{H.c.}) \\ &\times [d_{\mathbf{k}-\mathbf{q},\sigma}^{\dagger}(p_{x,\mathbf{k},\sigma}s_{x,\mathbf{k}} + p_{y,\mathbf{k},\sigma}s_{y,\mathbf{k}}) + \text{H.c.}], \end{aligned} \tag{10}$$

where we denote $s_{\alpha,\,\mathbf{k}} = \sin(k_{\alpha}a_{\alpha}/2)$. Next, following Shastry [38], we will define the "canonical" bosons and "canonical" fermions. As can be seen from Eq. (10), for the mode (7), (8) under consideration the canonical transformations of the operators $e_{\alpha,\mathbf{q}}^{\dagger}$ are similar in form to the transformations for the operators $p_{\alpha,\,\mathbf{k}}$, differing only by the sign:

$$\begin{aligned} b_{\mathbf{k}} &= \frac{i}{\mu_{\mathbf{k}}}(s_{x,\mathbf{k}}p_{x,\mathbf{k}} + s_{y,\mathbf{k}}p_{y,\mathbf{k}}), \\ a_{\mathbf{k}} &= \frac{i}{\mu_{\mathbf{k}}}(s_{y,\mathbf{k}}p_{x,\mathbf{k}} - s_{x,\mathbf{k}}p_{y,\mathbf{k}}) \end{aligned} \tag{11}$$

and

$$\begin{aligned} A_{\mathbf{q}} &= -\frac{i}{\mu_{\mathbf{q}}}(s_{x,\mathbf{q}}e_{x,\mathbf{q}} + s_{y,\mathbf{q}}e_{y,\mathbf{q}}), \\ B_{\mathbf{q}} &= -\frac{i}{\mu_{\mathbf{q}}}(s_{y,\mathbf{q}}e_{x,\mathbf{q}} - s_{x,\mathbf{q}}e_{y,\mathbf{q}}), \end{aligned} \tag{12}$$

where $\mu_{\mathbf{k}} = \sqrt{s_{x,\mathbf{k}}^2 + s_{y,\mathbf{k}}^2}$. The new bosonic and fermionic operators are centered on copper sites and satisfy the necessary commutation relations $[b_{\mathbf{k}}, a_{\mathbf{k}'}^{\dagger}]_+ = 0$ and $[B_{\mathbf{q}}, A_{\mathbf{k}'}^{\dagger}]_- = 0$. Making the corresponding substitutions, we will ultimately find

$$H_{pd}^{\text{epi}} = -2M_{pd}\sum_{\mathbf{k},\mathbf{q},\sigma} \mu_{\mathbf{k}}\mu_{\mathbf{q}}\varphi_{\mathbf{q}}^{A}(d_{\mathbf{k}+\mathbf{q},\sigma}^{\dagger}b_{\mathbf{k},\sigma} + \text{H.c.}), \tag{13}$$

where $\varphi_{\mathbf{q}}^{A} = (A_{-\mathbf{q}}^{\dagger} + A_{\mathbf{q}})$. As would be expected, the transformed Hamiltonian contains only one form of bosonic operators, the one that preserves the symmetry of the initial vibrational mode. In addition, in comparison with the previous version of the transformations [21, 22], the Wannier coefficient before the constant of the off-diagonal contribution changed in Eq. (13). These results distinguish the proposed formulation of the method from that realized previously in [21, 22].

Making similar transformations for the Hamiltonian H_{d}^{epi} describing the diagonal contribution to the EPI in Eq. (6), we will obtain

$$H_{d}^{\text{epi}} = M_{d}\sum_{\mathbf{k},\mathbf{q},\sigma} \mu_{\mathbf{q}}\varphi_{\mathbf{q}}^{A}(d_{\mathbf{k}+\mathbf{q},\sigma}^{\dagger}d_{\mathbf{k},\sigma} + \text{H.c.}). \tag{14}$$

Here, we took into account the fact that the energy of the holes on copper increases as the Cu–O bond length increases, with $M_{d} > 0$. Due to the symmetry of the vibrations, the off-diagonal coupling constant depends on both transferred momentum $\mathbf{q}$ and initial electron momentum $\mathbf{k}$, while the diagonal contribu-

tion a depends on the vector $\mathbf{q}$ only, which is consistent with the results of other authors [7, 40].

To rewrite the free-phonon Hamiltonian (5) $H^{\rm ph}$ in new variables (12), we will take into account the relation of the normal coordinate $Q_{\mathbf{g}}$ to the normal momentum $P_{\mathbf{g}}$, express each of the quantities $Q_{\mathbf{g}}$ and $P_{\mathbf{g}}$ in operators $e^{\dagger}_{\alpha,\mathbf{g}}(e_{\alpha,\ \mathbf{g}})$ and then in "canonical-boson" operators $A^{\dagger}_{\mathbf{q}}(A_{\mathbf{q}})$ and $B^{\dagger}_{\mathbf{q}}(B_{\mathbf{q}})$:

$$H^{\rm ph} = \sum_{\mathbf{q}} \hbar\omega\left[\left(A^{\dagger}_{\mathbf{q}}A_{\mathbf{q}} + \frac{1}{2}\right) + \left(B^{\dagger}_{\mathbf{q}}B_{\mathbf{q}} + \frac{1}{2}\right)\right]. \qquad (15)$$

It is important that the bosonic-excitation operators $B^{\dagger}_{\mathbf{q}}(B_{\mathbf{q}})$ are not mixed with any other excitations of the total Hamiltonian and, therefore, may be completely excluded from consideration.

The above transformations allow the Hamiltonians of the phonon system and the electron–phonon interaction to be broken down in the site representation into the local intracluster, $H_c^{\rm ph,epi}$, and intercluster, $H_{cc}^{\rm ph,epi}$, parts. For the electron Hamiltonian (2) we will immediately use the result of the corresponding transformations (11). As a result, the total Hamiltonian will be written as

$$H = H_c + H_{cc},$$
$$H_c = \sum_{\mathbf{g}} H_{\mathbf{g}}, \quad H_{cc} = \sum_{\mathbf{g},\mathbf{g}',\sigma} H_{\mathbf{g}\mathbf{g}',\sigma}, \qquad (16)$$

where the local contributions are

$$H^{\rm el}_{\mathbf{g}} = \sum_{\sigma}(\varepsilon_d - \mu)n^d_{\mathbf{g},\sigma} + \sum_{\sigma}(\varepsilon_b - \mu)n^b_{\mathbf{g},\sigma}$$
$$+ U_d n^d_{\mathbf{g},\sigma}n^d_{\mathbf{g},-\sigma} + U_b n^b_{\mathbf{g},\sigma}n^b_{\mathbf{g},-\sigma} + \sum_{\sigma,\sigma'} V_{bd}n^d_{\mathbf{g},\sigma}n^b_{\mathbf{g},\sigma'} \qquad (17)$$
$$- 2t_{pd}\mu_{00}\sum_{\sigma}(d^{\dagger}_{\mathbf{g},\sigma}b_{\mathbf{g},\sigma} + \text{H.c.}),$$

$$H^{\rm ph}_{\mathbf{g}} = \hbar\omega\left(A^{\dagger}_{\mathbf{g}}A_{\mathbf{g}} + \frac{1}{2}\right), \qquad (18)$$

$$H^{\rm epi}_{\mathbf{g}} = M_d\mu_{00}\sum_{\sigma}\varphi^A_{\mathbf{g}}n^d_{\mathbf{g},\sigma}$$
$$- 2M_{pd}\mu^2_{00}\sum_{\sigma}\varphi^A_{\mathbf{g}}(d^{\dagger}_{\mathbf{g},\sigma}b_{\mathbf{g},\sigma} + \text{H.c.}), \qquad (19)$$

while the intercluster part is defined as

$$H^{\rm el}_{\mathbf{g}\mathbf{g}',\sigma} = -2t_{pd}\mu_{\mathbf{g}\mathbf{g}'}(d^{+}_{\mathbf{g},\sigma}b_{\mathbf{g}',\sigma} + \text{H.c.})$$
$$- 2t_{pp}\nu_{\mathbf{g}\mathbf{g}'}b^{+}_{\mathbf{g},\sigma}b_{\mathbf{g}',\sigma}, \qquad (20)$$

$$H^{{\rm epi},d}_{\mathbf{g}\mathbf{g}',\sigma} = M_d\mu_{\mathbf{g}\mathbf{g}'}\varphi^A_{\mathbf{g}}n^{\sigma}_{\mathbf{g}'}, \qquad (21)$$

$$H^{{\rm epi},pd}_{\mathbf{g}\mathbf{g}',\sigma} = -2M_{pd}\sum_{\mathbf{h}}\mu_{\mathbf{g}\mathbf{g}'}\mu_{\mathbf{h}\mathbf{g}'}\varphi^A_{\mathbf{g}}(d^{\dagger}_{\mathbf{g}',\sigma}b_{\mathbf{h},\sigma} + \text{H.c.}). \qquad (22)$$

Here, we neglected the rapidly decreasing with distance intercluster contributions from the Coulomb matrix elements U_p and V_{pd} [36]. The Fourier transforms of the Wannier coefficients are given by the expressions

$$\mu_{\mathbf{g}\mathbf{g}'} = \frac{1}{N}\sum_{\mathbf{k}}\mu_{\mathbf{k}}\exp[-i\mathbf{k}(\mathbf{g} - \mathbf{g}')],$$

$$\nu_{\mathbf{g}\mathbf{g}'} = \frac{1}{N}\sum_{\mathbf{k}}\frac{4s^2_{x,\mathbf{k}}s^2_{y,\mathbf{k}}}{\mu^2_{\mathbf{k}}}\exp[-i\mathbf{k}(\mathbf{g} - \mathbf{g}')].$$

The proposed form of our analysis of the electron–phonon interaction in local variables allows the consideration of the strong electron correlation and EPI effects to be combined in a unified scheme of the generalized tight-binding method.

3. THE ROLE OF COMPETITION BETWEEN THE DIAGONAL AND OFF-DIAGONAL EPI FOR THE BREATHING MODE DURING THE FORMATION OF LOCAL CLUSTER STATES

In the scheme of the generalized tight-binding method the local cluster states determine the possible quasiparticle excitations that are a result of the transition from one state to another. Let us consider how the EPI strength affects the structure of the local states of correlated electrons. We will diagonalize the total Hamiltonian H_c for various configurations of copper and oxygen orbitals corresponding to an undoped compound with one hole per site (d^9p^6, $d^{10}p^5$) as well as to the cases with zero ($d^{10}p^6$) and two holes per site (d^9p^5, $d^{10}p^4$, and d^8p^6). Due to the electron–phonon interaction, each electronic state of the cluster is smeared into a set of polaron levels differing by the phonon "coat." For example, for a "vacuum" sector with the number of holes $n_h = 0$ the cluster eigenstates are

$$|0,\nu\rangle = |d^{10}p^6\rangle|\nu\rangle, \qquad (23a)$$

where $|\nu\rangle$ is a multiphonon state with the number of phonons $n_{\rm ph} = \nu$, For single-hole, $n_h = 1$, and two-hole, $n_h = 2$, sectors we will take into account only the lower polaron states formed by the spin doublet $|1\sigma\rangle$ and the singlet $|2\rangle$, respectively. Then,

$$|1\sigma,i\rangle = \sum_{\nu=0}^{N_{\max}}(c^d_{i,\nu}|d_{\sigma}\rangle + c^b_{i,\nu}|b_{\sigma}\rangle)|\nu\rangle, \qquad (23b)$$

$$|2,j\rangle = \sum_{\nu=0}^{N_{\max}}(c^{ZR}_{j,\nu}|ZR\rangle + c^{dd}_{j,\nu}|d_{-\sigma}d_{\sigma}\rangle + c^{bb}_{j,\nu}|b_{-\sigma}b_{\sigma}\rangle)|\nu\rangle. \qquad (23c)$$

Here,

$$|d_{\sigma}\rangle = d^{\dagger}_{\sigma}|0\rangle, \quad |b_{\sigma}\rangle = b^{\dagger}_{\sigma}|0\rangle,$$
$$|ZR\rangle = \frac{1}{\sqrt{2}}|d^{\dagger}_{-\sigma}b^{\dagger}_{\sigma} - d^{\dagger}_{\sigma}b^{\dagger}_{-\sigma}|0\rangle.$$

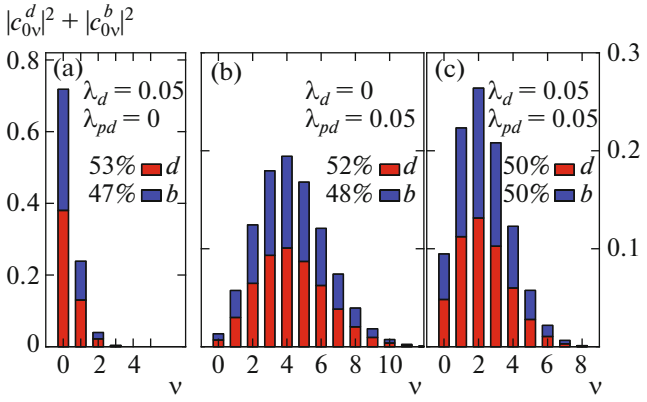

Fig. 1. (Color online) The structure of the ground state of local polarons in a single-particle sector, $n_h = 1$. The number of phonons ν is along the *x* axis; the total probability to find a hole with given ν, i.e., the sum of the squares of the amplitudes in Eq. (23b), is along the *y* axis.

The scheme of the local states is considered in detail in [21].

The parameters of the electron Hamiltonian H^{el} of the multiband *p*–*d* model (2) for La_2CuO_4 were obtained previously [41] by projecting [42] the electronic structure determined from first principles in the local electron density approximation onto the Wannier function basis. The corresponding parameters of the Hamiltonian H_c^{el} are given below. In contrast to the data of Table III from [42], we do not normalize the hopping integrals to t_{pd}. Thus,

$$\varepsilon_d = 0, \quad \varepsilon_p = 0.9, \quad \varepsilon_b = \varepsilon_p - 2t_{pp}\nu_{00} = 0.35,$$
$$t_{pp} = 0.86, \quad t_{pd} = 1.36$$

(all values are in electronvolts). The Coulomb matrix elements were taken from [43], where the electronic structure was fitted to the data of experimental angle-resolved photoemission spectroscopy (all in electronvolts):

$$U_d = 9, \quad U_p = 4, \quad U_b = U_p\Phi_{0000} = 0.84,$$
$$V_{pd} = 1.5, \quad V_{bd} = V_{pd}\Phi_{000} = 1.38.$$

Here, the coefficients Φ_{0000} and Φ_{000}, along with ν_{00} and μ_{00} from Eq. (17), describe the changes in the initial parameters of H^{el} when the molecular orbitals of neighboring clusters are orthogonolized [44].

We specify the EPI strength by the dimensionless parameter $\lambda_{d(pd)} = M^2_{d(pd)}/W\hbar\omega$, where the frequency of the planar breathing mode is $\hbar\omega = 0.09$ eV and W is the half-width of the free electron band. In the tight-binding method $W = zt$, where z is the coordination number; in our calculations $W = 2.15$ eV. Such a definition of the dimensionless coupling constant is often used in literature [24, 45, 46]. Basically, the parameter λ is the ratio of the energy of a localized electron in a deformed lattice to the kinetic energy of its delocalization [17].

According to Eqs. (23), the structure of the local polaron states (Fig. 1) is determined, first, by the electron density distribution in orbitals and, second, by the number of phonons ν from 0 to $N_{\max}$ involved in the formation of a polaron state at a given EPI strength. We do not fix $N_{\max}$ in our calculations in advance but defining it for a given EPI in such a way that the sum of the probabilities of the electron density distribution in all states with index ν is at least 99%. Third, the local states are characterized by a probability maximum of the electron density distribution in states with various numbers of phonons. According to these maxima, we call the states zero-phonon, single-phonon, etc., although the number of phonons is not a quantum number in this case.

Figure 1 shows the structure of the ground state of local polarons in a single-particle sector for various ratios of the diagonal and off-diagonal EPI parameters demonstrating their mutual influence.

As can be seen from a comparison of Figs. 1a and 1b, the diagonal EPI leads to much weaker renormalizations of the electronic states. For example, a state with a probability maximum at zero phonons is formed at $\lambda_d = 0.05$ and $\lambda_{pd} = 0$, while a multiphonon state with a probability maximum for $\nu = 4$ is realized in the opposite case ($\lambda_d = 0$ and $\lambda_{pd} = 0.05$). Figure 1c demonstrates a weakening of the off-diagonal contribution by the diagonal one, suggesting their competitive character. Note also the electron density redistribution with respect to the case without EPI: the diagonal and off-diagonal contributions lead to an increase in the population of copper and oxygen orbitals, respectively. The mutual influence of these contributions is responsible for the transition from a small local polaron to a large one.

Let us consider in detail how the competition between the diagonal and off-diagonal EPI affects the transition from zero-phonon states to multiphonon ones. Figure 2 shows a map of such transitions for the ground state in single-particle (Fig. 2a) and two-particle (Fig. 2b) sectors. The formation of multiphonon states due to the off-diagonal contribution, i.e., on the line $\lambda_d = 0$ to the right of the band of zero-phonon states, begins from $\lambda_{pd} \geq 0.025$ for $n_h = 1$ and from $\lambda_{pd} = 0.008$ for $n_h = 2$, while the diagonal contribution gives rise to multiphonon states only for λ_d larger by an order of magnitude, more specifically, at $\lambda_d \geq 0.3$ for $n_h = 1$ and $\lambda_d \geq 0.2$ for $n_h = 2$. Since the diagonal contribution is strongly suppressed by the off-diagonal one, the band of multiphonon states due to the diagonal contribution is realized in a very narrow range of the parameter λ_{pd} and cannot be displayed in the figure at a given scale. Thus, for the breathing mode the off-diagonal contribution is dominant, while its growth is conducive to a rapid shift in the probability of the elec-

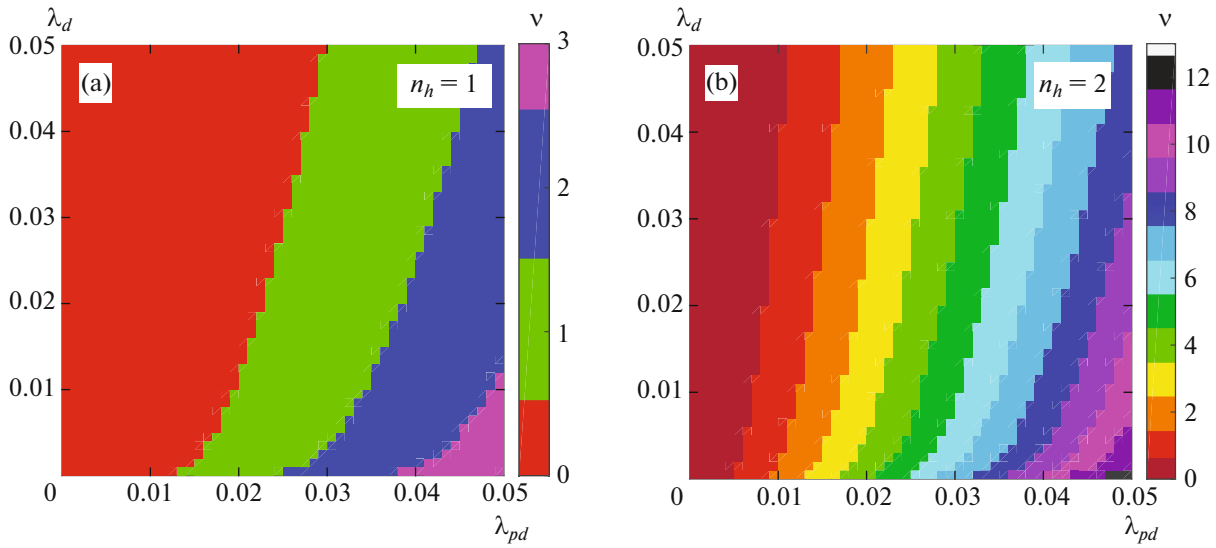

Fig. 2. (Color online) Influence of the EPI parameters on the position of the probability maximum in the electron density distribution in states with various numbers of phonons ν.

tron density distribution to states with a large number of phonons.

We also considered the influence of the Coulomb interaction U_d on the structure of local polaron states under conditions of strong EPI. For this purpose, we compared the maps of the transitions from zero-phonon states to multiphonon ones for the ground state in a two-particle sector at various values of the parameter U_d. The probability distributions in states with various numbers of phonons show that at a larger value of the local Coulomb interaction parameter the multiphonon states are realized for larger EPI parameters. For example, on the line $\lambda_d = 0$ the multiphonon states begin from $\lambda_{pd} = 0.008$ at $U_d = 9$ eV, from $\lambda_{pd} = 0.009$ at $U_d = 13$ eV, or from $\lambda_{pd} = 0.010$ at $U_d = 18$ eV. For the diagonal interaction the effect is more pronounced: on the line $\lambda_{pd} = 0$ the multiphonon states begin from $\lambda_d = 0.20$ at $U_d = 9$ eV, from $\lambda_d = 0.24$ at $U_d = 13$ eV, or from $\lambda_d = 0.26$ at $U_d = 18$ eV. Thus, during the formation of local polaron states the electron correlations suppress the EPI effects.

A comparison of the probability distributions in states with various numbers of phonons for single-particle and two-particle sectors at identical local Coulomb interaction parameters also suggests that the Coulomb interaction enhances the compensation of the diagonal contribution by the off-diagonal one. In other words, the suppression of EPI effects by electron correlations is more pronounced for the diagonal contribution. This can be explained by the fact that the local Coulomb correlations suppress the charge density fluctuations on copper, while the latter play a decisive role precisely in the diagonal EPI.

The mutual influence of strong electron correlations and strong EPI is one of the key problems of theoretically describing systems with SECs. Obviously, the result of interference between these interactions can differ not only for modes of different symmetries but also for different contributions from one mode. The approaches starting with a microscopic description are interesting from this viewpoint. Let us consider how the results obtained above correlate with the conclusions of other authors.

The authors of [13, 14] discussed the diagonal and off-diagonal EPI effects for a planar breathing mode based on the t–J model, i.e., for the quasiparticle excitations already formed by strong correlations. In this case, the diagonal interaction is related to the modulation of the Zhang–Rice singlet energy due to the changes in the set of parameters t_{pd}, ε_d, ε_p, and U_{pd}, while the off-diagonal contribution is determined by the modulation of the hopping parameter for the Zhang–Rice singlet (for comparison, see Eq. (6) and the reasoning before it). This description is valid for a weaker EPI and cannot be directly compared with the conclusions reached above. Nevertheless, note that by analyzing the superconducting pairing potential, the quasiparticle renormalizations, and the tunneling and optical spectra, the authors of [13] emphasize the decisive role of the off-diagonal contribution. This conclusion is retained not only in the regime of a Mott–Hubbard insulator, where the charge fluctuations are suppressed, but also in the regime of weak doping, where the EPI vertex renormalizations play a significant role.

It is worth noting that the matrix elements of the corresponding contributions were analyzed in [14]. Based on the assumptions about the distance dependence of the hopping, t_{pd}, and Coulomb interaction, V_{pd}, parameters, the authors showed the off-diagonal

matrix element to be much smaller than the diagonal one. However, this does not contradict our conclusions, because it can be seen from the above analysis that the role of the diagonal contribution during the formation of local polarons remains insignificant even for coupling parameters exceeding the off-diagonal contribution by an order of magnitude.

Finally, note [47], where the authors considered the EPI effects in a correlated system within the framework of a microscopic p–d model, and showed that the off-diagonal EPI with the breathing mode contributes significantly to the band renormalizations.

The conclusions about the dominant off-diagonal contribution are indirectly confirmed by the studies of the dynamic charge susceptibility in [48]. It was shown that the set of all experimental data could be explained only by assuming the interaction through the phonon field to be different in different parts of the Fermi surface, i.e., the electron–phonon coupling parameters depend on both transferred momentum $\mathbf{q}$ and wave vector $\mathbf{k}$. Such a dependence arises within the proposed approach only for the off-diagonal contribution, as can be seen from a comparison of Eqs. (13) and (14).

The authors of [49] investigated the influence of strong electron correlations on the renormalizations of the phonon spectra within a unified approach for various one-dimensional EPI models corresponding to the diagonal [1] and off-diagonal [50] types of interactions. Using the time-dependent Gutzwiller approximation, they showed that the phonon frequency renormalizations due to the diagonal contribution decrease with increasing local Coulomb interaction. This result complements the conclusions in [51] that for higher-dimensional systems electron–electron correlations effectively screen the electron coupling to the lattice and is consistent with our data on the suppression of EPI effects by Coulomb correlations.

Thus, the results obtained above correlate with the results of other authors and can serve as a starting point in choosing the way of describing the various properties of systems with strong electron correlations and strong EPI.

4. THE SCHEME FOR CALCULATING THE ELECTRONIC STRUCTURE IN THE POLARON VERSION OF THE GENERALIZED TIGHT-BINDING METHOD

After the diagonalization of the cluster Hamiltonian (17)–(19), the total Hamiltonian (17)–(22) can be rewritten in the Hubbard operators constructed on the basis of local polaron states $|0, \nu\rangle$, $|1, i\rangle$, and $|2, j\rangle$ according to the following rule:

$$Q_{\mathbf{g}} = \sum_{p,q} \langle p|Q_{\mathbf{g}}|q\rangle X_{\mathbf{g}}^{pq} = \sum_{m} \gamma^{m} X_{\mathbf{g}}^{m}. \qquad (24)$$

Here, $Q_{\mathbf{g}}$ is an arbitrary operator at site $\mathbf{g}$ and γ^m is the matrix element defining the probability of excitation from the initial state $|q\rangle$ to the final state $|p\rangle$ for a given mth pair of states. In the new representation the Fermi operators describe the quasiparticle hole, $X_{\mathbf{g}}^{2j,1i}$, and electron, $X_{\mathbf{g}}^{0\nu,1i}$, excitations that change the average number of phonons and the polarization of the oxygen environment of the copper atom.

When investigating the total Hamiltonian, we will exactly take into account the EPI effects due to the local intracluster contributions (18), (19) and will discard the intercluster EPI (21), (22) by noting that the Wannier coefficients $\mu_{\mathbf{gg}'}$ and $\nu_{\mathbf{gg}'}$ renormalizing it decrease rapidly with distance. We will obtain

$$H_c = \sum_{\mathbf{f},\nu} \varepsilon_{0\nu} Z_{\mathbf{f}}^{0\nu,0\nu} + \sum_{\mathbf{f},i} \varepsilon_{1i} Z_{\mathbf{f}}^{1i,1i} + \sum_{\mathbf{f},j} \varepsilon_{2j} Z_{\mathbf{f}}^{2j,2j},$$

$$H_{cc} = \sum_{\mathbf{f}\neq\mathbf{g},\sigma} \sum_{m,n} [-2t_{pp}\nu_{\mathbf{fg}}(\gamma_{b,\sigma}^{m})^{*}\gamma_{b,\sigma}^{n} \qquad (25)$$

$$- 2t_{pd}\mu_{\mathbf{fg}}((\gamma_{d,\sigma}^{m})^{*}\gamma_{b,\sigma}^{n} + (\gamma_{b,\sigma}^{m})^{*}\gamma_{d,\sigma}^{n})] X_{\mathbf{f}}^{\dagger m} X_{\mathbf{g}}^{n}.$$

Here, $Z_{\mathbf{f}}^{pp'}$ are the Bose Hubbard operators of local exciton excitations, occurring without any change in the number of holes in the initial and final states, and $\varepsilon_{0\nu}$, ε_{1i}, ε_{2j} are the energies of the many-electron and many-phonon eigenstates for a cluster with the number of holes $n_h = 0, 1, 2$, respectively. Note that, by definition, the matrix elements $\gamma_{d(b),\sigma}^{m}$ in the expression for H_{cc} contain the intracluster EPI effects.

According to Eq. (24), in the Hubbard operator representation the electron Green function

$$G_{\lambda\lambda',\sigma}(\mathbf{f},\mathbf{g};\omega) = \langle\langle a_{\mathbf{f}\lambda\sigma}|a_{\mathbf{g}\lambda'\sigma}^{\dagger}\rangle\rangle_{\omega}$$

with band indices $\lambda = b, d$ is expressed via the quasiparticle functions

$$D_{mn}(\mathbf{f},\mathbf{g};\omega) = \langle\langle X_{\mathbf{f}}^{m}|\, X_{\mathbf{g}}^{\dagger n}\rangle\rangle_{\omega}$$

by the relation

$$G_{\lambda\lambda',\sigma}(\mathbf{f},\mathbf{g};\omega) = \sum_{m,n} \gamma_{\lambda,\sigma}^{m}(\gamma_{\lambda',\sigma}^{n})^{*} D_{mn}(\mathbf{f},\mathbf{g};\omega). \qquad (26)$$

The expressions for the quasiparticle Green functions were derived in a generalized Hartree–Fock approximation using a procedure like the Mori projection technique [52, 53]. In this approach the zero Green function in the Dyson equation contains static spatial correlation functions that renormalize significantly the spectrum of Hubbard excitations [54–57]. As a

result, the dispersion equation for quasiparticles appears as follows:

$$\det\|(\omega-\Omega_m)\delta_{mn}-F_m t_{mn}(\mathbf{k})-\Sigma_{mn}(\mathbf{k})\|=0. \quad (27)$$

Note that the indices m and n number the quasiparticle excitations, while the indices in parentheses, for example, (zw), specify these excitations directly as the transitions between the corresponding states z and w. The quantity $\Omega_m \equiv \Omega_{(pq)} = \varepsilon_q - \varepsilon_p$ defines the quasiparticle excitation energy. The coefficients $F_m \equiv F_{(pq)} = \langle Z^{pp}\rangle + \langle Z^{qq}\rangle$ depend on the average occupation numbers of the initial and final states and are called the occupation factors. The elements $t_{mn}(\mathbf{k})$ of the intercluster hopping matrix are

$$t_{mn}(\mathbf{k}) = -\frac{2}{N}\sum_{(\mathbf{f}-\mathbf{g}),\sigma} e^{i\mathbf{k}\cdot(\mathbf{f}-\mathbf{g})}[t_{pp}\nu_{\mathbf{fg}}(\gamma^m_{b,\sigma})^*\gamma^n_{b,\sigma} + t_{pd}\mu_{\mathbf{fg}}((\gamma^m_{d,\sigma})^*\gamma^n_{b,\sigma} + (\gamma^m_{b,\sigma})^*\gamma^n_{d,\sigma})]. \quad (28)$$

The contribution of the spin correlation functions is specified by the elements of the matrix $\Sigma_{mn}(\mathbf{k}) = \Sigma_{(uv),(zw)}(\mathbf{k})$:

$$\Sigma_{(uv),(zw)}(\mathbf{k}) = \frac{2}{F_{(zw)}} \times \sum_{\mathbf{k}',\sigma} \begin{cases} \sum_{p,s} t_{(pu)(zs)}(\mathbf{k}')c^{(pv)(ws)}_{\mathbf{k}'}, \Leftrightarrow n^u_h = 0, \quad n^z_h = 0, \\ \sum_{p,r} t_{(pu)(rw)}(\mathbf{k}')c^{(pv)(rz)}_{\mathbf{k}'}, \Leftrightarrow n^u_h = 0, \quad n^z_h = 1, \\ \sum_{q,s} t_{(vq)(zs)}(\mathbf{k}')c^{(uq)(ws)}_{\mathbf{k}'}, \Leftrightarrow n^u_h = 1, \quad n^z_h = 0, \\ \sum_{q,r} t_{(vq)(rw)}(\mathbf{k}')c^{(uq)(rz)}_{\mathbf{k}'}, \Leftrightarrow n^u_h = 1, \quad n^z_h = 1. \end{cases}$$

Here, the eigenfunctions are sorted out in such a way that the number of holes n_h in the u, z, q, and s states is one less than that in the v, w, p, and r states. In addition, the p and v (or w and s) states in the structure of the spin correlation function $c^{(pv)(ws)}_{\mathbf{k}}$ have opposite spin projections. We will take into account the correlators constructed only on the ground single-hole states and assume that an isotropic spin liquid state with a short-range antiferromagnetic order is realized in the system. In this case, the Fourier transforms of the spin correlation functions are

$$c^{(pv)(ws)}_{\mathbf{k}} = \sum_{\mathbf{f},\mathbf{g}}\langle X^{pv}_{\mathbf{f}} X^{ws}_{\mathbf{g}}\rangle e^{i\mathbf{k}\cdot(\mathbf{f}-\mathbf{g})} = \sum_{\mathbf{f},\mathbf{g}}\langle X^{\sigma\bar{\sigma}}_{\mathbf{f}} X^{\bar{\sigma}\sigma}_{\mathbf{g}}\rangle e^{i\mathbf{k}\cdot(\mathbf{f}-\mathbf{g})} = 2\sum_{\mathbf{f},\mathbf{g}}\langle S^z_{\mathbf{f}} S^z_{\mathbf{g}}\rangle e^{i\mathbf{k}\cdot(\mathbf{f}-\mathbf{g})}, \quad (29)$$

where $\bar{\sigma} = -\sigma$.

The presence of an occupation factor in Eq. (27) leads to temperature dependences of the band structure and the spectral weight of quasiparticles [58]. This effect for systems with strong electron correlations has been demonstrated previously using the $LaCoO_3$ compound as an example, where the strong temperature dependence of the occupation numbers is due to the crossover between the low-spin and high-spin Co^{+3} states. The occupation of single-hole eigenstates in a cluster at room temperature is specified by the Boltzmann distribution

$$n_{1,i} = n_{1,i=0}\exp\left[-\frac{\varepsilon_{1,i}-\varepsilon_{1,i=0}}{kT}\right]. \quad (30)$$

At $T = 0$ K only the excitations involving an occupied ground state have a nonzero spectral weight. The occupation of the ground state decreases with rising temperature, while the occupation of the first, second, and succeeding excited states increases in accordance with Eq. (30). For example, at $T = 800$ K the occupation is significant up to the seventh excited state:

$$n_0 = 0.42, \quad n_1 = 0.24, \quad n_2 = 0.14, \quad n_3 = 0.08,$$
$$n_4 = 0.02, \quad n_5 = 0.01, \quad n_6 = 0.007, \quad n_7 = 0.003.$$

Note that we disregard the anharmonic effects whose role increases with temperature and, therefore, the results presented below for high temperatures are qualitative.

5. THE BAND STRUCTURE AND THE SPECTRAL WEIGHT OF POLARONS AT FINITE TEMPERATURES

The band structure of quasiparticle excitations in a system with strong electron correlations and strong EPI consists of the Hubbard fermion bands split into subbands as a result of their hybridization with multiphonon Franck–Condon resonances. Both diagonal and off-diagonal EPI lead to splittings of the coherent excitation band in a certain energy range and to the spectral weight transfer to high-energy multiphonon excitations with a weak dispersion. The electron–phonon coupling strength affects the number and degree of splittings, the spectral weight distribution between multiphonon excitations. The loss of spectral weight and dispersion smearing suggest a partial loss of quasiparticle coherence. In other words, the quasiparticles are defined more poorly. The effect from the diagonal EPI is seen to be much smaller (Fig. 3a) than that from the off-diagonal one (Fig. 3b). In the case of diagonal EPI with $\lambda_d = 0.025$, a weak splitting into subbands occurs in the conduction band; the valence band is barely affected (Fig. 3a). In the case of off-diagonal EPI ($\lambda_{pd} = 0.025$), the energy ranges where the interaction with multiphonon excitations destroys the coherence of the band-forming quasiparticles are clearly distinguished in the conduction and valence bands (Fig. 3b). The simultaneous presence of diagonal and off-diagonal EPI is accompanied by their partial compensation. In the regime of equal diagonal and off-diagonal EPI, the diagonal EPI reduces the effect

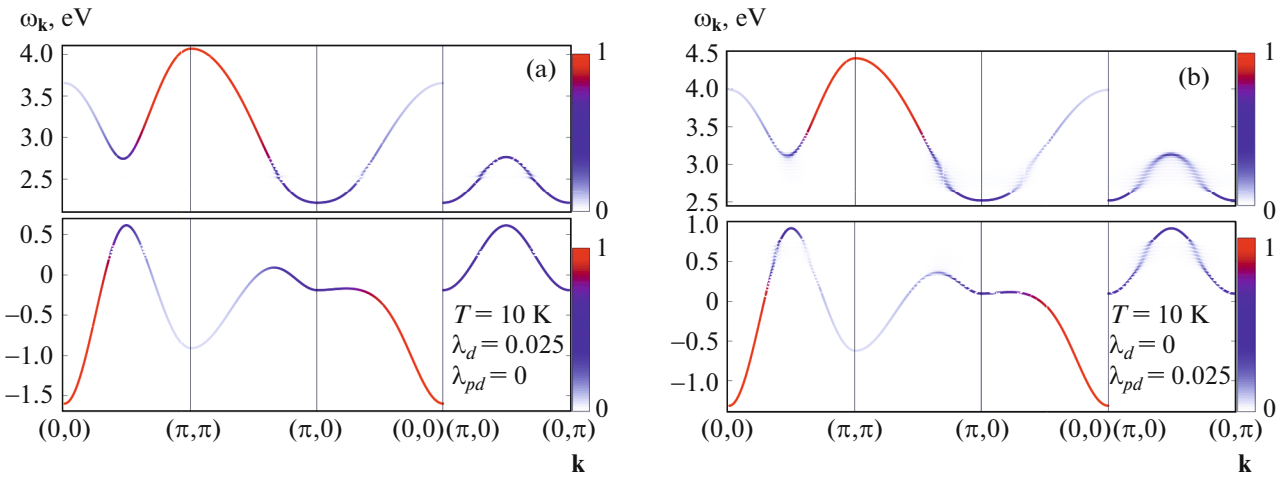

Fig. 3. (Color online) The band structure of Hubbard polarons when only the diagonal (a) and off-diagonal (b) EPI are taken into account for temperature $T = 10$ K. The upper and lower parts of the figure show the conduction and valence bands, respectively. The color at each point of the dispersion dependence characterizes the spectral intensity of a quasiparticle excitation with given $\mathbf{k}$ and $\omega_{\mathbf{k}}$ on the relative scale shown on the right.

from the off-diagonal EPI to a small degree, the highest-energy excitations lose their spectral weight, and the splittings in the wide Hubbard fermion band are closed at the energies of these excitations (Fig. 4a). On the whole, the dispersion of low-energy excitations in the case of equal diagonal and off-diagonal EPI remains the same as that in the case of only off-diagonal EPI.

As the temperature rises, the quasiparticles constructed with the involvement of occupied single-hole excited states acquire dispersion and spectral weight. We can separate the contributions to the dispersion reconstruction with increasing temperature from the N–N excitations without any change of the local state number and the N–N' excitations with a change of the polaron state number. The N–N excitations are involved in the formation of a split-off subband in the upper part of the valence band and in the lower part of the conduction band. The multiphonon N–N' excitations form subbands as a result of the Hubbard fermion band splittings, as do the multiphonon 0–N' excitations. The contribution of the N–N excitations to the temperature dependence of the electronic structure is retained even at zero EPI. Without EPI the N–N excitations are phonon-free excitations (transitions between local states with the same number of phonons). The multiphonon N–N' excitations (transitions with a change of the number of phonons) without EPI have zero intensity due to the absence of an overlap between the initial and final phonon states.

A rise in temperature causes a reconstruction of the split-off band and a smearing of the valence and conduction bands in the region of existence of multiphonon excitations with a nonzero spectral weight (Fig. 4). The reconstruction of the split-off valence band consists predominantly in the growth of the electronic excitation energy at points (0, 0) and (π, π). In contrast, the energy decreases for low-intensity excitations in the remaining lower part of the valence band in the vicinity of point (π, π). Flat bands, more intense at point (π, π) and less intense at point (0, 0), are formed at $T = 400$ K at points (0, 0) and (π, π) of the split-off band (Fig. 4b). Owing to the presence of flat bands, the density of states at $T = 400$ K has a peak at energy $\omega \approx 0.763$ eV (Fig. 5, the red line), in contrast to the monotonic dependence at $T = 10$ K (Fig. 5, the black line). As the temperature rises further, the local maximum at point (π/2, π/2) becomes a local minimum, i.e., the split-off band of N–N excitations is turned upside down (see Fig. 4c, $T = 600$ K), taking a form typical for the dispersion in the paramagnetic phase with a low-intensity maximum at point (0, 0) and a high-intensity maximum at point (π, π) (see Fig. 4d, $T = 800$ K). In this case, the flat band reaches the valence band top. For small EPI constants the valence band top at all temperatures is formed by coherent excitations, the region of incoherent multiphonon excitations with the largest spectral weight lies below in energy. At $\lambda_d = \lambda_{pd} = 0.025$ the boundary of the smearing region almost coincides with the energy of the flat band of coherent excitations at temperatures above $T = 400$ K. On the whole, a rise in temperature leads to an increase in the width of the valence and conduction bands and to their shift characterized by a decrease in the dielectric gap.

The dispersion smearing at the energies of the most intense multiphonon excitations includes the growth of the Hubbard fermion band splittings, the decrease in the slope of the dispersion curve, and the spectral weight redistribution. The splitting of the Hubbard fermion band into several subbands increases as a result of additional hybridization with multiphonon

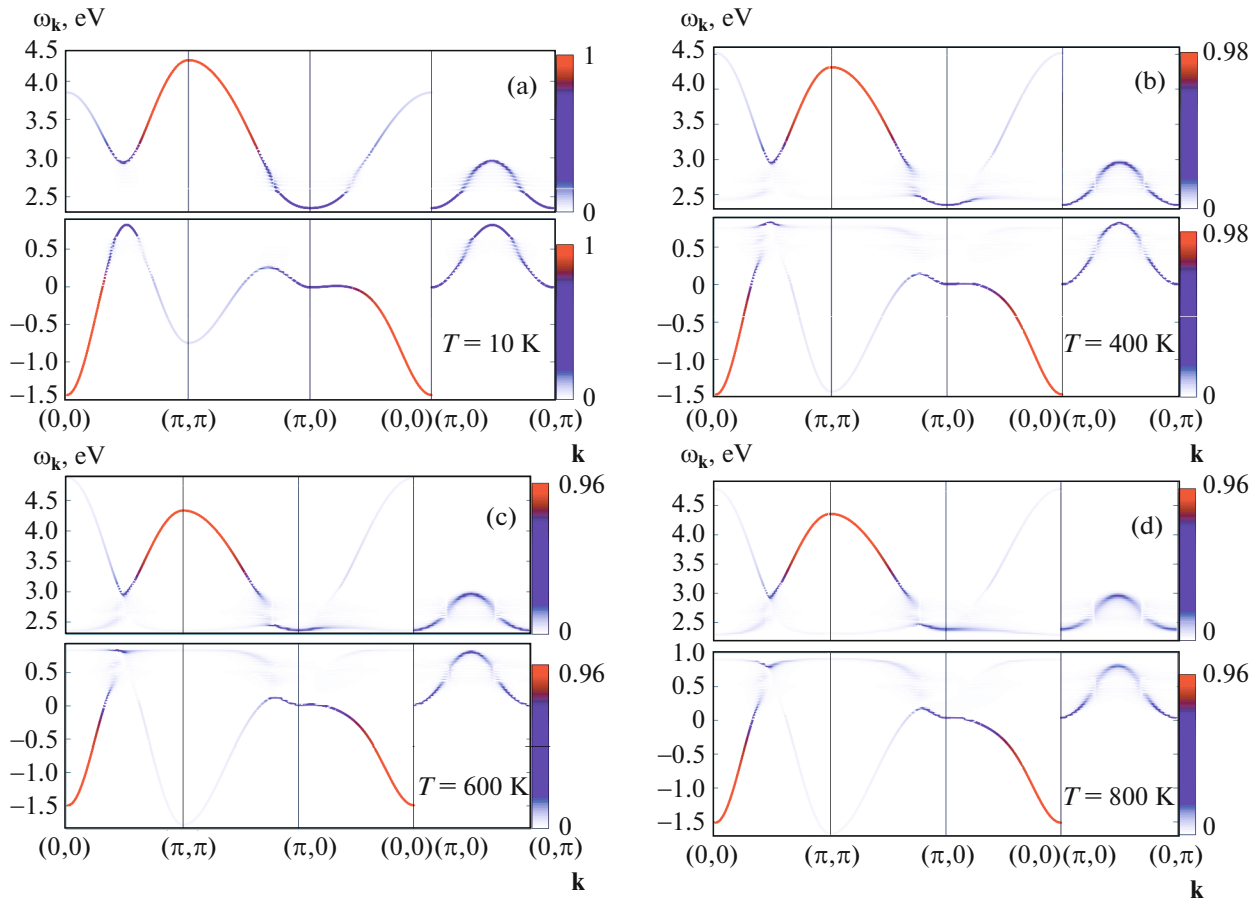

Fig. 4. (Color online) Evolution of the band structure of Hubbard polarons as the temperature increases from 10 to 800 K in the regime of weak EPI at $\lambda_d = \lambda_{pd} = 0.025$. At $T = 400$, 600, and 800 K a flat band is clearly seen in the vicinity of points $\mathbf{k} = (\pi, \pi)$ and (0, 0).

N–N' excitations having energies close to those of 0–N'' excitations. In this case, the dispersion of each subband becomes weaker with increases temperature in the vicinity of the splitting points, the slope of the dispersion curve becomes smaller, and the segment of the Hubbard fermion band gradually turns into a flat band (see Figs. 4b–4d). The spectral weight is distributed more uniformly over the points in k-space in each subband. Thus, in the energy range from 0.25 to 0.75 eV of the valence band (and from 2.5 to 3 eV of the conduction band) a rise in temperature turns the high-intensity coherent excitations with wave vectors within a certain range into slow and heavy polaron quasiparticles will all possible wave vectors. The smearing region grows with rising temperature; at $T = 800$ K its size is 0.8 eV in the valence band (and 0.9 eV in the conduction band).

The spectral function of quasiparticle excitations

$$A(\mathbf{k},\omega) = \left(-\frac{1}{\pi}\right)\sum_{\lambda,\sigma;m,n}\gamma^{m}_{\lambda,\sigma}(\gamma^{n}_{\lambda,\sigma})^{*}\,\mathrm{Im}\langle\langle X^{m}_{\mathbf{k}}|X^{\dagger n}_{\mathbf{k}}\rangle\rangle_{\omega+i\delta} \quad (31)$$

and its temperature dependence depend significantly on the wave vector. We will analyze the spectral function at point $(\pi/2, \pi/2)$ in k-space, because the most dramatic temperature effect, a broadening of the peak of the lower Hubbard band, was revealed in the experiments on angle-resolved photoemission spectroscopy precisely at this point. At a low temperature $T = 10$ K for $\lambda_d = \lambda_{pd} = 0.025$ the spectral function at point $(\pi/2, \pi/2)$ consists of a high-intensity 0–0 excitation peak and low-intensity peaks of multiphonon excitations (Fig. 6a). The rise in temperature from 10 to 400 K does not lead to a significant increase in the intensity of multiphonon excitations. The spectral weight redistribution when the excited local polaron states are occupied becomes more noticeable as the temperature increases further ($T = 600$ K, Fig. 6b); the 0–0 peak loses its intensity, while the multiphonon peaks, on the contrary, become more intense. Due to the reconstruction of the split-off subband, the 0–0 peak approaches the multiphonon peaks and at high temperatures falls into the smearing region of the valence band by N–N' excitations ($T = 800$ K, Fig. 6c). The hybridization of 0–0 and N–N' excitations is accom-

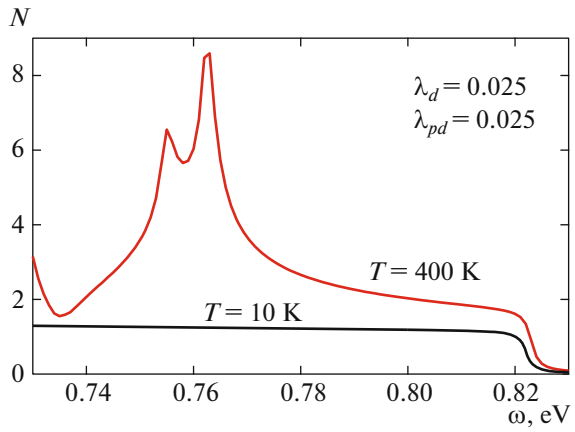

Fig. 5. (Color online) The density of states $N(\omega)$ of Hubbard polarons at the valence band top at $T = 10$ K (black line) and 400 K (red line) in the regime of weak EPI. The highest peak at $T = 400$ K is attributable to the presence of a flat band near points (0, 0) and (π, π).

panied by an additional redistribution of the spectral weight between them. As a result, it becomes impossible to associate each peak of the spectral function with a specific Franck–Condon process, the quasiparticle excitations are a superposition of various multiphonon processes with similar weights. In this case, the spectral function is a wide distribution of peaks. When the finite lifetime of quasi-particle excitations is taken into account by increasing the Lorentzian width δ = 0.03 eV, the distribution of peaks merges into a single wide peak. The rise in temperature from 10 to 400 K does not lead to an increase in the width of the peak of the spectral function at point ($\pi/2$, $\pi/2$) (Fig. 6d). As the temperature rises from 400 to 800 K, the full width at half maximum of the peak, Γ_{FWHM}, increases by more than half.

At large EPI constants the region where the wide Hubbard fermion bands are split into Hubbard polaron subbands grows. At $\lambda_d = \lambda_{pd} = 0.1$ the conduction and valence bands are split in the energy interval of 0.8 eV (Fig. 7a); this interval becomes larger with

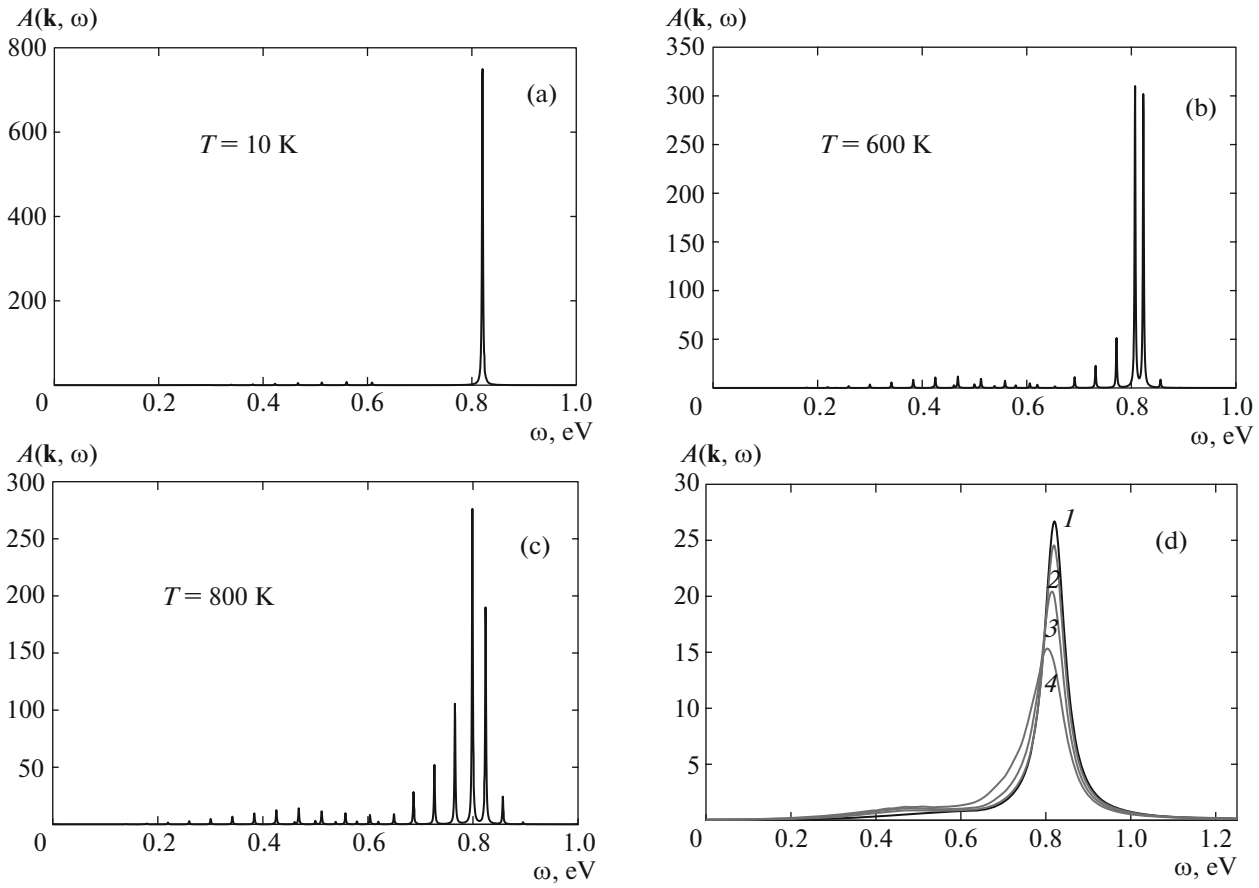

Fig. 6. (Color online) (a–c) Evolution of the spectral function of Hubbard polarons as the temperature increases from 10 to 800 K in the regime of weak EPI at point $\mathbf{k} = (\pi/2, \pi/2)$; $\lambda_d = \lambda_{pd} = 0.025$. The calculations were performed for the Lorentzian width $\delta = 0.001$ eV. (d) The broadening of the spectral function with rising temperature at $\delta = 0.03$ eV at the same point for the same λ_d and λ_{pd}: $T = 10$ K, $\Gamma_{\text{FWHM}} = 0.06$ eV (curve *1*); $T = 400$ K, $\Gamma_{\text{FWHM}} = 0.06$ eV (curve *2*); $T = 600$ K, $\Gamma_{\text{FWHM}} = 0.07$ eV (curve *3*); $T = 800$ K, $\Gamma_{\text{FWHM}} = 0.1$ eV (curve *4*).

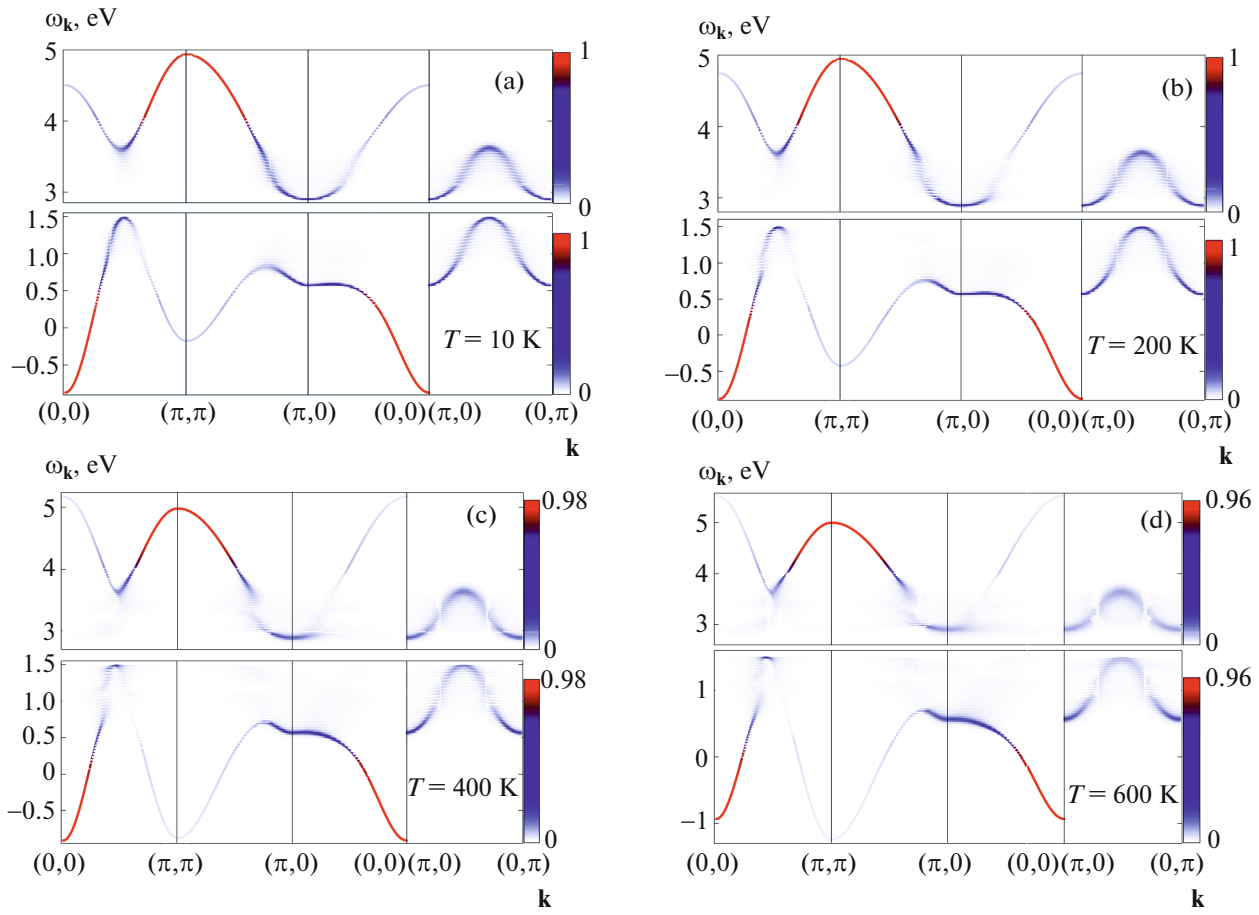

Fig. 7. (Color online) Evolution of the band structure of Hubbard polarons as the temperature rises from 10 to 600 K in the regime of strong EPI at $\lambda_d = \lambda_{pd} = 0.1$. At $T = 400$ and 600 K the flat band in the vicinity of points $\mathbf{k} = (0, 0)$ and $\mathbf{k} = (\pi, \pi)$ breaks up into a set of less intense flat subbands of polaron excitations.

rising temperature. The spectral weight is distributed over all weakly dispersive subbands and over all quasiparticles inside each subband. The quasiparticles in wide regions of the k-space whose shape follows that of the Hubbard fermion bands at zero EPI constants remain more intense, i.e., the dispersion of the Hubbard fermion band is also retained at strong EPI if it is traced by the maxima of the spectral function. The spectral function of the valence band at point $(\pi/2, \pi/2)$ is characterized by a wide distribution of low-intensity peaks of quasiparticles, which are a superposition of multiphonon Franck–Condon 0–N excitations, already at low temperatures (Fig. 8a). However, the FWHM of the peak of the spectral function at a low temperature and $\lambda_d = \lambda_{pd} = 0.1$ (for the Lorentzian width $\delta = 0.03$ eV), $\Gamma^{0.1}_{\text{FWHM}} = 0.07$ eV differs only slightly from that at EPI constants $\lambda_d = \lambda_{pd} = 0.025$ ($\Gamma^{0.025}_{\text{FWHM}} = 0.06$ eV).

As the temperature rises, the transformation of the split-off band manifests itself as a redistribution of the spectral weight inside the Hubbard subbands. This transformation occurs against the background of a reconstruction of the Hubbard subbands, the spectral weight redistribution between various subbands and between valence band inside each subband (see Fig. 7) caused by the occupation of excited local polaron states with temperature. For large EPI constants the spectral weight redistribution is stronger with rising temperature. Therefore, the dispersion of the Hubbard bands is strongly smeared at high temperatures, the valence band top (and the conduction band bottom) consists of weakly dispersive polaron subbands with a spectral weight distributed uniformly over all points of the Brillouin zone (see Fig. 7d).

A significant redistribution of the spectral weight between Hubbard polarons for large EPI constants manifests itself as a broadening of the distribution of peaks in the spectral function and a change in the shape of their envelope (Figs. 8b and 8c). As the temperature increases from 10 to 400 K, the FWHM of the peak constructed for the Lorentzian width $\delta = 0.03$ eV almost doubles and is $\Gamma_{\text{FWHM}} = 0.13$ eV (Fig. 8d). The calculated broadening agrees in order of magnitude

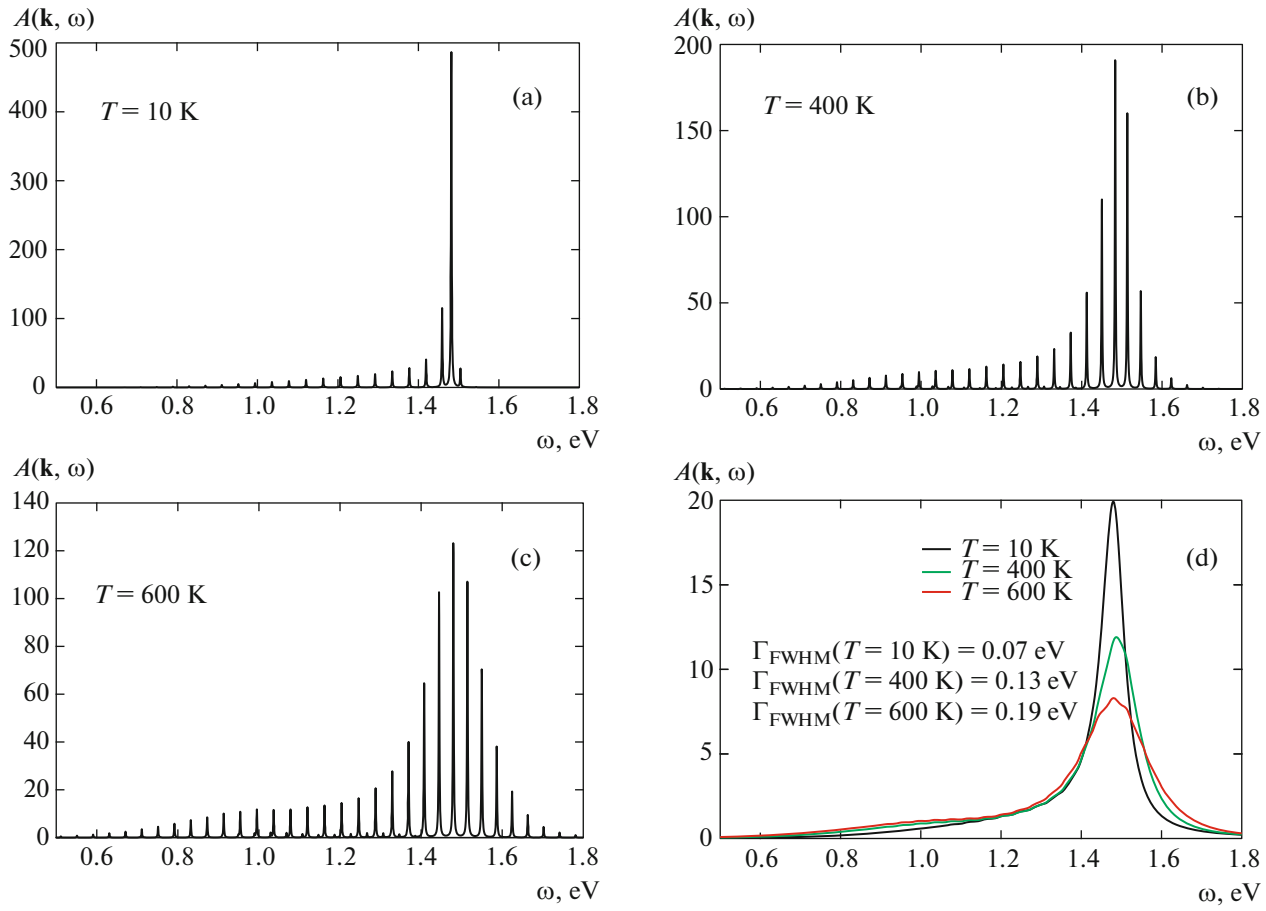

Fig. 8. (Color online) (a)–(c) Evolution of the spectral function of Hubbard polarons at point $\mathbf{k} = (\pi/2, \pi/2)$ as the temperature increases from 10 to 600 K in the regime of strong EPI at $\lambda_d = \lambda_{pd} = 0.1$. The calculations were performed for the Lorentzian width $\delta = 0.001$ eV. (d) The broadening of the spectral function at the same point with rising temperature at $\delta = 0.003$ eV and $\lambda_d = \lambda_{pd} = 0.1$.

with the broadening of the spectra measured by angle-resolved photoemission spectroscopy: in the experiment the increase in temperature from 200 to 400 K is accompanied by an increase in the FWHM of the peak of the lower Hubbard band by a factor of 2. In the temperature range from 10 to 600 K the FWHM of the peak increases by more than a factor of 2.5 (Fig. 8d). Thus, it can be seen that the degree of broadening and the change in the shape of the peak with temperature are largely governed by the EPI strength.

6. CONCLUSIONS

In this paper we corrected the formulation of the polaron version of the generalized tight-binding method. We considered the mutual influence of the electron correlations and electron–phonon interaction for the breathing mode within the proposed approach by taking into account the microscopic peculiarities of the structure of the material. Subsequently, this will allow us to describe the polarons formed under conditions of simultaneously strong Coulomb and electron–phonon interactions using effective low-energy models. Based on the polaron version of the generalized tight-binding method, we considered the competition between the diagonal and off-diagonal contributions in the interaction of correlated CuO-plane electrons with breathing mode vibrations. We showed that during the formation of local polaron states, (1) the off-diagonal contribution due to the modulation of the oxygen–copper hopping integral is predominant; (2) in addition, the Coulomb interaction suppresses the EPI effects, weakening the influence of the diagonal contribution to a greater extent. Thus, the off-diagonal EPI with the breathing mode plays a major role in forming the quasiparticle excitations of Hubbard polarons.

We also reached similar conclusions about the role of these contributions and their relationship when investigating the electronic structure of the systems under consideration. A strong EPI leads to the loss of quasiparticle excitation coherence, with the transformation of the band structure being determined predominantly by the off-diagonal contribution.

We demonstrated a number of important effects. First, the band structure of Hubbard polarons has a strong temperature dependence. For ordinary electronic bands the temperature effects are weak, because the characteristic electronic excitation energies are great compared to the thermal energy. For Hubbard polarons the situation is different, because the Franck–Condon resonance energy is comparable to the thermal one. This leads to the strong reconstruction of the dispersion and the spectral function of Hubbard polarons described above.

Second, we showed that the temperature dependence of the band structure for strongly correlated systems based on copper oxides is characterized by a gradual evolution from the antiferromagnetic dispersion with the valence band top at point $(\pi/2, \pi/2)$ at low temperatures to the paramagnetic dispersion with the valence band top at point (π, π) at high temperatures. At intermediate temperatures a narrow flat band, which gives a sharp peak in the density of states in the vicinity of room temperature, splits off at the valence band top. The spectral functions of the polarons at the valence band top broaden with decreasing amplitude as the temperature rises, in qualitative agreement with the photoelectron spectra.

ACKNOWLEDGMENTS

We are grateful to V.I. Zinenko and V.A. Gavrichkov for useful discussions. This work was financially supported by the Russian Foundation for Basic Research (project no. 16-02-00098) and the Basic Research Program no. 12 of the Presidium of the Russian Academy of Sciences ("Fundamental Problems of High-Temperature Superconductivity").

REFERENCES

1. T. Holstein, Ann. Phys. **8**, 325 (1959).
2. T. Holstein, Ann. Phys. **8**, 343 (1959).
3. H. Frolich, Adv. Phys. **3**, 325 (1954).
4. A. L. Kuzemsky, A. Holas, and N. M. Plakida, Phys. B (Amsterdam, Neth.) 122, 168 (1983).
5. T. P. Devereaux, A. Virosztek, and A. Zawadowski, Phys. Rev. B **51**, 505 (1995).
6. J. Song and J. F. Annett, Phys. Rev. B **51**, 3840 (1995).
7. N. Bulut and D. J. Scalapino, Phys. Rev. B **54**, 14971 (1996).
8. T. Sakai, D. Poilblanc, and D. J. Scalapino, Phys. Rev. B **55**, 8445 (1997).
9. A. S. Alexandrov and P. E. Kornilovitch, Phys. Rev. Lett. **82**, 807 (1999).
10. E. G. Maksimov, Phys. Usp. **43**, 965 (2000).
11. H. Fehske, J. Loos, and G. Wellein, Phys. Rev. B **61**, 8016 (2000).
12. J. Bonča and S. A. Trugman, Phys. Rev. B **64**, 094507 (2001).
13. S. Ishihara and N. Nagaosa, Phys. Rev. B **69**, 144520 (2004).
14. O. Rösch and O. Gunnarsson, Phys. Rev. Lett. **92**, 146403 (2004).
15. A. S. Mishchenko and N. Nagaosa, Phys. Rev. Lett. **93**, 036402 (2004).
16. G. Sangiovanni, O. Gunnarsson, E. Koch, et al., Phys. Rev. Lett. **97**, 046404 (2006).
17. C. Slezak, A. Macridin, G. A. Sawatzky, et al., Phys. Rev. B **73**, 205122 (2006).
18. N. M. Plakida and V. S. Oudovenko, J. Supercond. Nov. Magn. **29**, 1037 (2016).
19. S. G. Ovchinnikov and E. I. Shneder, J. Exp. Theor. Phys. **101**, 844 (2005).
20. E. I. Shneyder, J. Spitaler, E. E. Kokorina, et al., J. Alloys Compd. **648**, 258 (2015).
21. I. A. Makarov, E. I. Shneyder, P. A. Kozlov, et al., Phys. Rev. B **92**, 155143 (2015).
22. P. Piekarz, J. Konior, and J. H. Jefferson, Phys. Rev. B **59**, 14697 (1999).
23. O. Gunnarsson and O. Rösch, J. Phys.: Condens. Matter **20**, 043201 (2008).
24. A. S. Mishchenko, Phys. Usp. **52**, 1193 (2009).
25. N. Gedik, D.-S. Yang, G. Logvenov, et al., Science (Washington, DC, U. S.) **316**, 425 (2007).
26. L. Pintschovius, Phys. Status Solidi B **242**, 30 (2005).
27. T. Cuk, D. H. Lu, X. J. Zhou, et al., Phys. Status Solidi B **242**, 11 (2005).
28. D. Reznik, Adv. Condens. Matter Phys. **2010**, 523549 (2010).
29. C. L. Fu and A. J. Freeman, Phys. Rev. B **35**, 8861 (1987).
30. W. Weber and L. F. Mattheis, Phys. Rev. B **37**, 599(R) (1988).
31. F. Giustino, M. L. Cohen, and S. G. Louie, Nature (London, U.K.) **452**, 975 (2008).
32. R. E. Cohen, W. E. Pickett, and H. Krakauer, Phys. Rev. Lett. **62**, 831 (1989).
33. E. I. Shneyder and S. G. Ovchinnikov, JETP Lett. **83**, 394 (2006).
34. D. Zech, H. Keller, K. Conder, et al., Nature (London, U.K.) **371**, 681 (1994).
35. P. I. Arseev and N. S. Maslova, Phys. Usp. **53**, 1151 (2010).
36. V. A. Gavrichkov, S. G. Ovchinnikov, A. A. Borisov, and E. G. Goryachev, J. Exp. Theor. Phys. **91**, 369 (2000).
37. S. G. Ovchinnikov, V. A. Gavrichkov, M. M. Korshunov, et al., Springer Ser. Solid-State Sci. **171**, 143 (2012).
38. B. S. Shastry, Phys. Rev. Lett. **63**, 1288 (1989).
39. A. S. Davydov, *Solid State Theory*, Ed. by D. A. Mirtova (Nauka, Moscow, 1976).
40. S. Barišić, Phys. Rev. B **5**, 932 (1972).
41. M. M. Korshunov, V. A. Gavrichkov, S. G. Ovchinnikov, et al., Phys. Rev. B **72**, 165104 (2005).
42. V. I. Anisimov, D. E. Kondakov, I. A. Nekrasov, et al., Phys. Rev. B **71**, 125119 (2005).
43. B. Wells, Z.-X. Shen, A. Matsuura, et al., Phys. Rev. Lett. **74**, 964 (1995).

44. L. F. Feiner, J. H. Jefferson, and P. Raimondi, Phys. Rev. B **53**, 8751 (1993).
45. P. E. Kornilovitch, Phys. Rev. Lett. **81**, 5382 (1998).
46. L.-C. Ku, S. A. Trugman, and J. Bonča, Phys. Rev. B **65**, 174306 (2002).
47. T. P. Devereaux, T. Cuk, Z.-X. Shen, et al., Phys. Rev. Lett. **93**, 117004 (2004).
48. M. V. Eremin and M. A. Malakhov, JETP Lett. **100**, 324 (2014).
49. E. von Oelsen, A. di Ciolo, J. Lorenzana, et al., Phys. Rev. B **81**, 155116 (2010).
50. W. P. Su, J. R. Schrieffer, and A. J. Heeger, Phys. Rev. B **22**, 2099 (1980).
51. A. di Ciolo, J. Lorenzana, M. Grilli, et al., Phys. Rev. B **79**, 085101 (2009).
52. H. Mori, Prog. Theor. Phys. **34**, 399 (1965).
53. N. Plakida, Springer Ser. Solid-State Sci. **171**, 173 (2012).
54. N. M. Plakida and V. S. Oudovenko, J. Exp. Theor. Phys. **104**, 230 (2007).
55. A. F. Barabanov, A. A. Kovalev, O. V. Urazaev, A. M. Belemuk, and R. Hayn, J. Exp. Theor. Phys. **92**, 677 (2001).
56. V. V. Val'kov and D. M. Dzebisashvili, J. Exp. Theor. Phys. **100**, 608 (2005).
57. S. G. Ovchinnikov, M. M. Korshunov, and E. I. Shneyder, J. Exp. Theor. Phys. **109**, 775 (2009).
58. S. G. Ovchinnikov, Yu. S. Orlov, I. A. Nekrasov, and Z. V. Pchelkina, J. Exp. Theor. Phys. **112**, 140 (2011).

Translated by V. Astakhov